Improved evaluation of antivascular cancer therapy using constrained tracer-kinetic modeling for multiagent dynamic contrast-enhanced MRI

Improved evaluation of antivascular cancer therapy using constrained tracer-kinetic modeling for multi-agent dynamic contrast-enhanced MRI

Stefanie J Hectors[1,2,#], Igor Jacobs[1,3,#], Jasper Lok[4], Johannes Peters[4], Johan Bussink[4], Freek J Hoeben[5], Henk M Keizer[5], Henk M Janssen[5], Klaas Nicolay[1,†], Matthias C Schabel[6], Gustav J Strijkers[1,7,*]

[1] Biomedical NMR, Department of Biomedical Engineering, Eindhoven, The Netherlands

[2] Translational and Molecular Imaging Institute, Icahn School of Medicine at Mount Sinai, New York, NY, USA

[3] Oncology Solutions, Philips Research, Eindhoven, The Netherlands

[4] Department of Radiation Oncology, Radboud University Medical Center, Nijmegen, The Netherlands

[5] SyMO-Chem BV, Eindhoven, The Netherlands

[6] Advanced Imaging Research Center, Oregon Health & Science University, Portland, OR, USA

[7] Biomedical Engineering and Physics, Academic Medical Center, University of Amsterdam, Amsterdam, The Netherlands

[#] These authors contributed equally to this work; [†] Deceased January 10th 2017

* Corresponding author
Gustav Strijkers
Academic Medical Center
Meibergdreef 9
1105 AZ Amsterdam
g.j.strijkers@amc.uva.nl

The authors have no conflicts of interest.

Keywords: dendrimeric contrast agents; macromolecular DCE-MRI; anti-vascular therapy; vascular disrupting agents; tracer-kinetic modeling

Running title: Multi-agent DCE-MRI for evaluation of antivascular therapy

Word count: 3812
Number of references: 35
Number of figures: 4
Number of tables: 0

Abstract

Dynamic contrast-enhanced MRI (DCE-MRI) is a promising technique for assessing the response of tumor vasculature to anti-vascular therapies. Multi-agent DCE-MRI employs a combination of low and high molecular weight contrast agents, which potentially improves the accuracy of estimation of tumor hemodynamic and vascular permeability parameters. In this study, we employed multi-agent DCE-MRI to assess changes in tumor hemodynamics and vascular permeability after vascular-disrupting therapy. Multi-agent DCE-MRI (sequential injection of G5 dendrimer, G2 dendrimer, and Gd-DOTA) was performed in tumor-bearing mice before, 2 h and 24 h after treatment with vascular disrupting agent DMXAA or placebo. Constrained DCE-MRI gamma capillary transit time modeling was employed to estimate flow F, blood volume fraction v_b, mean capillary transit time t_c, bolus arrival time t_d, extracellular extravascular fraction v_e, vascular heterogeneity index α^{-1} (all identical between agents) and extraction fraction E (reflective of permeability) and transfer constant K^{trans} (both agent-specific) in perfused pixels. F, v_b, and α^{-1} decreased at both time points after DMXAA, while t_c increased. E (G2 and G5) showed an initial increase after which both parameters restored. K^{trans} (G2 and Gd-DOTA) decreased at both time points after treatment. In the control, placebo-treated animals, only F, t_c, and K^{trans} Gd-DOTA showed significant changes. Histological perfused tumor fraction was significantly lower in DMXAA-treated versus control animals. Our results show how multi-agent tracer-kinetic modeling can accurately determine the effects of vascular-disrupting therapy, by separating simultaneous changes in tumor hemodynamics and vascular permeability.

Introduction

During early development of anti-vascular cancer drugs, a number of treatment effects are commonly investigated, including the mechanism of drug action, required dose, optimal therapy scheduling, and therapeutic efficacy (1, 2). Functional imaging techniques can provide quantitative imaging biomarkers to enable early assessment of treatment effects. Dynamic contrast-enhanced magnetic resonance imaging (DCE-MRI), predominantly using low molecular weight contrast agents, is widely applied in both preclinical and clinical studies for noninvasive and longitudinal monitoring of anti-vascular therapies (1-3). Tracer-kinetic modeling can be performed to calculate pharmacokinetic parameters that reflect microvascular functionality (4-6). One of the most commonly used tracer-kinetic parameters is the transfer constant K^{trans} from the model introduced by Tofts and Kermode (hereafter named the Tofts model), which describes the transfer rate of contrast material from the intravascular space into the tumor interstitial space (7-9). Typically, a reduction in K^{trans} is observed after anti-vascular therapy, providing useful information on therapeutic effects (1, 2). However, K^{trans} is a composite measure that is influenced by both blood flow and microvascular permeability (10). These effects can often not be separately determined, since many anti-vascular therapies induce changes in both of these parameters. As an example, vascular targeting therapies can cause increased microvascular permeability due to vascular disruption along with decreased blood flow due to vascular collapse and hemorrhage (11-13). Several studies have shown that macromolecular contrast agents may be more sensitive to changes in microvascular permeability and blood volume (14, 15) and that low molecular weight and macromolecular agents could be combined to

obtain an improved assessment of tracer-kinetic parameters (16-18). However, a more detailed modeling approach may be required to fully identify the various vascular changes upon treatment.

Recently we employed a multi-agent DCE-MRI approach, in which contrast agents of various molecular weight [generation 5 (G5) and generation 2 (G2) poly(propolyene imine) (PPI) dendrimers functionalized with Gd-DOTA moieties and low-molecular weight contrast agent Gd-DOTA] were sequentially injected within one imaging session in non-treated tumor-bearing mice (19). Simultaneous modeling of the multi-agent DCE-MRI data was performed, for which a number of hemodynamic parameters, including blood flow, were constrained to be identical between the different boluses, whereas tracer-kinetic parameters related to microvascular permeability were separately determined for each agent. It was demonstrated that the hemodynamic parameters could be separately determined from vascular permeability using this approach. In addition, a contrast agent size-dependent decrease in the extraction fraction was measured, reflecting the lower degree of vascular permeability for macromolecular contrast agents. It was hypothesized that this approach can be used to evaluate the various changes in these tracer-kinetic parameters upon treatment targeting the vasculature.

The purpose of the present study was to apply this new multi-agent DCE-MRI method in a therapeutic setting and investigate whether it can provide a detailed assessment of changes in both hemodynamic parameters and microvascular permeability after vascular disrupting therapy of tumors in mice with the model drug DMXAA.

Methods

Ethics Statement

All animal experiments in this prospective study were performed according to the Directive 2010/63/EU of the European Commission and approved by the Animal Care and Use Committee of Maastricht University, The Netherlands.

Animal model

12-14 week-old BALB/cByJ mice (Charles River Laboratories, Sulzfeld, Germany) were inoculated with $1x10^6$ CT26.WT mouse colon carcinoma cells (CRL-2638, American Type Culture Collection, Manassas, VA, United States) subcutaneously in their right hind limb. Approximately 10 days after inoculation, tumors became palpable in all animals.

Study design

Baseline MRI measurements were performed 1 day before either anti-vascular treatment (n=13) or placebo treatment (n=16). Subsequently, mice were randomly assigned to one of these treatment groups. Mice in the anti-vascular treatment group were intraperitoneally injected with the vascular disrupting agent 5,6-Dimethylxanthenone-4-acetic acid (DMXAA, Sigma-Aldrich, St. Louis, MO, USA), freshly prepared at a dose of 20 mg/kg DMXAA dissolved in 5% sodium bicarbonate in ultrapure water (0.5 mg DMXAA / 100 µL). This agent was used as a model therapeutic agent, since the vascular shutdown by DMXAA is known to result from increased permeability (20). Mice in the placebo treatment group were intraperitoneally injected with an equivalent volume of 5% sodium bicarbonate in ultrapure water. At 2 h after either DMXAA (n=13) or

placebo (n=16) treatment, mice underwent post-treatment MRI measurements. After the 2 h post-treatment MRI measurements, some of the animals (DMXAA n=6, placebo n=8) were sacrificed. The remaining animals additionally underwent MRI at 24 hours after DMXAA (n=7) or placebo (n=8) treatment and were subsequently sacrificed.

Contrast agents for multi-agent DCE-MRI

Multi-agent DCE-MRI measurements were performed using contrast agents with a range of molecular weights. Modified PPI dendrimers, functionalized with Gd-DOTA moieties via a polyethylene glycol (PEG) spacer, were synthesized by SyMO-Chem BV (Eindhoven, The Netherlands). These agents comprised a high molecular weight (59517 Da) generation 5 dendrimer (G5-PPI-$(PEG_6$-GdDOTA$)_{64}$) and an intermediate molecular weight (7317 Da) generation 2 dendrimer (G2-PPI-$(PEG_6$-GdDOTA$)_8$). In addition to these macromolecular agents, the clinically available low molecular weight (754 Da) gadoterate meglumine (Gd-DOTA, Dotarem®, Guerbet, Villepinte, France) was used. Contrast agent relaxivity in Balb/c mouse serum (Innovative Research, Novi, MI, United States) was measured at 7 T and 37°C. Additional information on synthesis and characterization of the dendrimer-based contrast agents is provided in the **Supplementary Information** with additional figures and a table showing results of the dendrimer characterization (**Supplementary Figure S1:** synthesis schemes of the G2 and G5 dendrimers; **Supplementary Figures S2:** mass spectroscopy spectrum of the PPI building blocks; **Supplementary Figure S3:** mass spectroscopy spectrum of G2 and gel permeation chromatography spectrums of the G2 and G5 dendrimers; **Supplementary Figure S4:** size measurements of the G2 and G5 dendrimers using dynamic light scattering; **Supplementary Table S1:** longitudinal (r_1) and transverse (r_2)

MRI relaxivity values of GdDOTA, G2 and G5). The dendrimer-based contrast agents were dissolved in phosphate-buffered saline. For contrast agent administration, an infusion line was filled with equal volumes of the G5 dendrimer, G2 dendrimer and Gd-DOTA (at a concentration of 125 mM, ~0.1 mmol/kg), separated by equal volumes of saline. Small air bubbles between each volume prevented mixing of the agents. The gadolinium concentrations of the solutions used in the in vivo experiments were determined with inductively coupled plasma-optical emission spectrometry and the injected volumes were corrected for small differences in the actual concentration.

MRI acquisition and analysis

Animal preparation

Mice were anesthetized using isoflurane (3% for induction and 1-2% for maintenance) in medical air (at a flow rate of 0.4 L/min). A tail vein catheter for contrast agent injections was placed, after which the mice were positioned in a custom made cradle, equipped with an anesthesia mask and warm water circuit to maintain body temperature at 37°C. MRI measurements were performed with a 7T Bruker BioSpec 70/30 USR (Bruker BioSpin MRI GmbH, Ettlingen, Germany) equipped with a 1H 59/35 (outer/inner diameter in mm) circular polarized MRI transceiver volume coil (Bruker BioSpin MRI GmbH, Ettlingen, Germany). During MRI measurements, respiration rate was monitored using a balloon pressure sensor and temperature with a rectal temperature probe.

B_0 and B_1 calibration.

First, local shimming of the tumor was performed. Thereafter, anatomical reference T_2-weighted images were acquired using a three-dimensional turbo rapid acquisition with

relaxation enhancement (RARE) sequence. Sequence parameters were: repetition time/effective echo time = 2000/34.4 ms, flip angle = 90°, field of view = 30x30x24 mm^3, acquisition matrix = 75x75x16, and RARE factor = 8. In order to correct for local inhomogeneities in the radiofrequency field, B_1 mapping was performed with the 180° signal null method (21) using a gradient-spoiled and radiofrequency-spoiled three-dimensional T_1-weighted fast low-angle shot (FLASH) sequence. The flip angles of the global excitation pulses were centered around 180° (flip angles = 120°, 150°, 180°, 210°, 240°). Other sequence parameters were: repetition time/echo time = 100/3.03 ms, field of view = 30x30x48 mm^3, and acquisition matrix = 56x42x26 reconstructed to 75x75x32. Only the center slices, corresponding to the anatomical T_2-weighted images, were selected for further analysis. Data were fitted to determine the nominal flip angle required for signal nulling, from which the B_1-correction factors were calculated.

T_1 mapping

The longitudinal relaxation time T_1 before contrast agent injection was derived from T_1-weighted images that were acquired using a gradient-spoiled and radiofrequency-spoiled three-dimensional FLASH sequence with variable flip angles. Detailed sequence parameters were: repetition time/echo time = 1.38/0.69 ms, flip angles = 1°, 2°, 3°, 5°, 7°, 10°, 13°, 20°, field of view = 30x30x24 mm^3, acquisition matrix = 50x39x14, reconstructed to 75x75x16, and 15 repetitions. Only repetitions 8-15, at which a steady-state signal intensity was obtained, were used for further analysis. B_1 inhomogeneity correction was performed by multiplication of the flip angles by B_1 correction factors in each pixel. Non-linear regression of the variable flip angle T_1-mapping data was

performed using the standard spoiled-gradient echo signal-equation to determine the pre-contrast T_1 values for each voxel.

Multi-agent DCE-MRI

Multi-agent DCE-MRI measurements were performed using the same sequence and sequence parameters as for pre-contrast T_1 mapping, with a flip angle of 15° and 730 repetitions, resulting in a temporal resolution of 0.82 s and total acquisition time of 10 min. Contrast agent injections were performed at 1 (G5 dendrimer), 4 (G2 dendrimer) and 7 (gadoterate meglumine) min after start of the acquisition, using an infusion pump (Chemyx Fusion 100, Stafford, TX, United States) at a rate of 2 mL/min. B_1-corrected dynamic ΔR_1 ($=1/\Delta T_1$) values were calculated for each voxel based on the standard spoiled gradient-echo signal-equation, using the pre-contrast T_1 values and post-contrast dynamic signal intensities. Regions of interest delineating the tumor were manually drawn using the anatomical T_2-weighted images.

Multi-agent tracer-kinetic modeling

Details of the multi-agent tracer-kinetic modeling have been described in our previously published work (19). In short, arterial input functions (AIF) were determined for each agent separately using the Monte Carlo Blind Estimation algorithm (22, 23) applied to the ΔR_1 curves of tumor voxels that exhibited significant perfusion. A pixel was considered perfused if the mean ΔR_1 between the first and second contrast agent injection was higher than 2 times the standard deviation of ΔR_1 before contrast injection. The DCE-MRI derived perfused fraction (PF) was calculated from this analysis. Multi-agent curves in the perfused pixels were simultaneously fitted with the gamma capillary

transit time (GCTT) model (24). This model characterizes contrast uptake curves with six model parameters: blood flow F, extraction fraction E [i.e. the fraction of contrast agent molecules that leak into the extravascular extracellular space (EES), reflective of vascular permeability], washout rate constant k_{ep} of the contrast agent molecules from EES to intravascular space, mean capillary transit time t_c, bolus arrival time t_d and vascular heterogeneity index α^{-1}, the latter representing the width of the distribution of t_c within a tissue voxel. In principle, each bolus of injected contrast agent could be separately fitted, resulting in 18 model parameters. By imposing physiological constraints, four of these six parameters (F, t_c, t_d and α^{-1}) were identical between the different boluses, while E and k_{ep} were separately determined for each contrast agent. From the estimated parameters transfer constant $K^{trans} = E*F$, extravascular extracellular volume fraction $v_e = E*F/k_{ep}$ and blood volume fraction $v_b = F*t_c$ were derived. The latter three parameters, K^{trans}, v_e and v_b, are all estimated parameters that are described in the conventionally used extended Tofts model (9). As indicated earlier, K^{trans} is a composite measure of vascular permeability and blood flow. Only the perfused pixels were included in the DCE-MRI fitting, because the parameters cannot be accurately determined in pixels that do not exhibit significant enhancement. Median tumor parameter values for each measurement were calculated for each MRI examination.

Histological analysis

After the MRI measurements, a subset of mice [2 h after placebo (n=4), 24 h after placebo (n=4), 2 h after DMXAA (n=3), 24 h after DMXAA (n=4)] was injected with bisBenzimide H 33342 trihydrochloride (Hoechst, Sigma-Aldrich) as a perfusion marker.

For the Hoechst staining, mice were kept anesthetized after the MRI measurement and Hoechst (8 mg/mL in saline, 32 mg/kg) was injected via the tail vein. After 3 min, mice were sacrificed by cervical dislocation. Further processing of the tumor tissue is described in the **Supplementary Information**. In short, the frozen tumor sections were subsequently stained for endothelial cells. Semi-automated analysis of the stained slides was performed to determine perfused vessel fractions (PF) from the Hoechst staining and vascular density (VD) from the endothelial staining.

Statistical analysis

Data are presented as mean ± standard deviation (SD). Statistical analysis was performed in SPSS (version 20, IBM, Armonk, NY). Normality of the tracer-kinetic DCE-MRI parameter values and histopathological data in the different groups was confirmed using a Kolmogorov Smirnov test ($P>0.315$) and subsequently parametric tests were used for the statistical analyses. Linear mixed models were used to assess whether the multi-agent DCE-MRI parameters significantly changed over time in the DMXAA-treated and placebo-treated animal groups. If a certain parameter showed significant differences over time, the parameter values were compared between the different time points using Bonferroni-corrected two-sided t-tests. The quantitative histological measurements between DMXAA-treated and placebo treated animals were compared using two-sided Student t-tests. For all tests, a P-value lower than 0.05 was considered significant.

Results

Representative multi-agent DCE-MRI parameter maps of a DMXAA-treated and placebo-treated animal are shown in **Figures 1** and **2**, respectively. While the DCE-MRI parameters overall remained stable in the placebo-treated animals, substantial treatment effects were observed in the parameter maps of the DMXAA-treated animals. Both at 2 h and at 24 h after treatment a large region of the tumor was non-perfused. In the remaining perfused pixels of the tumor, substantially decreased flow was observed at 2 h and at 24 h. In addition, a pronounced increase in permeability was observed at 2 h, as expressed by an increase in the extraction fraction E of G5 and G2 and to a lesser extent in the extraction fraction of Gd-DOTA. The increase in permeability was not reflected in the K^{trans} maps. K^{trans} of G2 and G5 did not show visual differences in the perfused pixels upon treatment, while K^{trans} of Gd-DOTA showed a decrease at both time points after treatment.

The mean quantitative DCE-MRI parameters of the perfused pixels at the different time points are presented in **Figure 3**. In the placebo-treated animals most of the parameters did not significantly change over time, except for a mild, yet significant, decrease in F and K^{trans} Gd-DOTA at both time points after placebo treatment ($P<0.005$ and $P<0.016$, respectively) and an increase in t_c at 2 h after treatment ($P=0.008$). In the DMXAA-treated animals, at 2 h and 24 h after treatment most parameters were significantly different from baseline. From the hemodynamic parameters that are non-contrast-agent specific, PF ($P<0.001$), F ($P<0.001$), v_b ($P<0.001$) and α^{-1} ($P<0.001$) significantly decreased at both time points after the DMXAA treatment compared to baseline measurements, while t_c significantly increased at both post-treatment time points

($P<0.040$). The DMXAA treatment did not induce significant changes in v_e ($P>0.082$). The changes in contrast-agent-specific DCE-MRI parameters after DMXAA treatment were markedly different among the contrast agents. E G5 initially strongly increased at 2 h after DMXAA treatment ($P<0.001$), whereupon it significantly dropped again at 24 h ($P<0.001$). E G2 also significantly increased at 2 h after DMXAA treatment ($P=0.003$), after which its value seemed to drop again at 24 h, yet not significantly with respect to the 2 h time point ($P=0.206$). E Gd-DOTA did not show significant change upon DMXAA treatment. Finally, K^{trans} G5 did not change upon treatment, while both K^{trans} G2 and K^{trans} Gd-DOTA significantly decreased at both post-treatment time points ($P<0.024$ and $P<0.001$, respectively).

The histopathological results from Hoechst perfusion measurements are shown in **Figure 4A-B**. DMXAA-treated animals exhibited large regions of non-perfused tissue in histology. Histological PF was significantly lower for the DMXAA-treated animals at both time points after treatment compared to the placebo-treated animals at the same time points ($P<0.005$). VD from histology was not significantly different between the DMXAA-treated and control animals ($P>0.094$).

Discussion

In this paper, we presented the first application of a recently developed multi-agent tracer-kinetic modeling approach (19) for the assessment of tumor treatment response. Sequential injection of different contrast agents has been employed previously for evaluation of tumor vascular properties using DCE-MRI (17, 18, 25-27). However, in these previous studies the different injections were separately analyzed, while simultaneous modeling of the multi-agent data facilitates a comprehensive and robust assessment of tissue properties by exploiting the fact that a number of parameters can be constrained to be identical between the agents based on physiological grounds (19).

The vascular disrupting agent DMXAA was chosen as model agent for the assessment of anti-vascular therapy. DMXAA (also known as Vadimezan and ASA404) induces a cascade of anti-vascular events in the tumor early after administration (13, 28). Within 30 minutes after administration it induces endothelial cell apoptosis, leading to increased vascular permeability and decreased blood perfusion, resulting from loss of plasma and associated higher blood viscosity (28). The subsequent loss of endothelial barrier causes increased vascular permeability (20). A second mechanism of action of DMXAA is the induction of tumor necrosis factor alpha (TNFα) among other cytokines (28). TNFα contributes to increase in vascular permeability (29). The enhanced permeability causes an increase in interstitial pressure, which further compromises tumor blood flow (30). Generally, in mouse models this cascade of events completely shuts down the tumor vasculature, after a transient period of decreased blood flow and high vascular permeability. In clinical trials with DMXAA in patients the anti-vascular cascade was observed only partly, with minor increase in TNFα after DMXAA administration (13).

Because of the limited therapeutic effects in patients, the development of DMXAA has been discontinued in 2010 after unsuccessful Phase III trials, in which no effects of DMXAA on overall survival could be proven (31). Nevertheless, DMXAA remains an interesting drug to investigate in the preclinical setting because of its well-defined anti-vascular effects, which can be used to investigate novel imaging methods for the characterization of tumor vasculature, as was done in the present study.

The here observed effects of treatment on DCE-MRI parameters are exactly in line with the previously described vascular events following administration of DMXAA. The rapid drop in PF, F and v_b is consistent with induction of endothelial apoptosis and subsequent vascular shutdown early after administration. The increase in t_c at both time points after treatment is likely related to high blood viscosity and associated low blood flow. The significant drop in α^{-1} after treatment is indicative of a narrower distribution of t_c in the tumor pixels and a lower vascular heterogeneity. A possible explanation for this finding is that the response of blood vessels to the vascular therapy depends on the blood flow (28). Vessels with low blood flow may be particularly sensitive to vascular disrupting agents (28). The DMXAA may thus have particularly affected these blood vessels, leading to immediate vascular shutdown. Removal of these specific capillary paths by DMXAA treatment may have resulted in the observed more homogeneous distribution of capillary transit times in the remaining perfused vasculature. Next to the overall diminished blood flow, we observed a transient increase in permeability (E G2 and E G5) at 2 h, which dropped again at 24 h after treatment. This finding is in agreement with endothelial barrier loss and increased vascular permeability after DMXAA treatment. The

drop in vascular permeability at 24 h after treatment could be a result from increased interstitial pressure (30).

An important result of this study is that the increase in permeability would not have been detected using only a low molecular weight contrast agent, such as Gd-DOTA, as we did not observe an increase in E Gd-DOTA at 2 h after DMXAA treatment. This finding further advocates the use of high molecular weight contrast agents for characterization of tumor vasculature (14). Moreover, the use of differently sized contrast agents in the same acquisition can give additional insights in the vascular permeability, such as the endothelial pore size (3). Our results also further stress that a more complete insight in vascular changes can be obtained from advanced modeling of macromolecular DCE-MRI data, compared to conventional Tofts modeling. K^{trans} of G2 and G5 both failed to show an increase in permeability after treatment, because of the counteracting effects of decreased flow and increased permeability on K^{trans} (10).

In the placebo-treated control animals generally no changes in DCE-MRI parameters were observed over time, except for a decrease in F and K^{trans} Gd-DOTA and increase in t_c. The reduction in tumor perfusion may be related to the repeated anesthesia. It has previously been shown that repeated isoflurane anesthesia leads to a decreased heart rate and blood pressure in rats (32), although we have not confirmed this by monitoring of heart rate and blood pressure for the mice in this study. This systemic physiological effect of anesthesia likely also influences the local blood flow in the tumor tissue.

The histopathological results from Hoechst staining corroborated the DCE-MRI findings. While the number of vessels was similar between DMXAA- and placebo-treated animals,

there was a significant drop in the histology-derived PF in the DMXAA-treated animals, similar as seen in DCE-MRI.

While we employed multi-agent tracer-kinetic modeling for assessment of vascular effects after treatment with a vascular disrupting agent, this method could also be used for evaluation of other anti-vascular therapies. The technique could be particularly useful for characterization of the dynamic effects of anti-angiogenic therapies on the tumor vasculature. Anti-angiogenic agents may induce transient normalization of the tumor vasculature, prior to vascular shutdown (33). Vessel normalization is characterized by reduction of the abnormal tortuosity and hyperpermeability of tumor blood vessels, leading to reduced interstitial pressure and increased blood flow (34). This transient period of vessel normalization can be exploited by combination therapies of anti-angiogenic and cytotoxic agents (34). For full efficacy of these combination therapies it is important to optimize the treatment schedule and dosing. While Tofts modeling may not be sensitive enough for detection of vessel normalization, because of the counteracting effects of higher blood flow and lower permeability on K^{trans}, the multi-agent approach, combined with a more sophisticated model of the tissue microvasculature (such as the GCTT model used here), is able to differentiate between these effects and is therefore probably more suitable for evaluation of anti-angiogenic therapies.

Whereas the application of the multi-agent tracer-kinetic modeling is mainly focused on the preclinical evaluation of tumor vasculature, it is also relevant to humans. Recently, the feasibility of clinical application of the multi-agent modeling approach has been shown in patients with (high risk of) pancreatic cancer (35). It was shown that the multi-

agent approach is promising for the identification of pancreatic malignancies. In that particular study, the injection protocol consisted of sequential injection of low-molecular weight gadoteridol and the iron-based nanoparticle blood pool agent ferumoxytol.

Our study had some limitations. Only one vascular therapeutic agent was evaluated. The sensitivity of the technique to the vascular effects of other therapeutic agents needs to be assessed in future studies. In addition, the method was only tested in one animal tumor model. While we expect that the method is translatable to other animal models as well as to human applications, future studies in different cancer models are needed to further validate the use of the multi-agent tracer-kinetic modeling technique for assessment of anti-vascular therapies.

In conclusion, we have shown that multi-agent tracer-kinetic modeling can be used to accurately determine the effects of a vascular disrupting agent on the tumor vasculature. The technique could separate simultaneous effects on tumor hemodynamics and vascular permeability, while conventional DCE-MRI failed to discriminate between these vascular changes.

References

1. O'Connor JP, Jackson A, Parker GJ, Roberts C, Jayson GC. Dynamic contrast-enhanced MRI in clinical trials of antivascular therapies. Nat Rev Clin Oncol. 2012 Mar;9(3):167-77.

2. Zweifel M, Padhani AR. Perfusion MRI in the early clinical development of antivascular drugs: decorations or decision making tools? Eur J Nucl Med Mol Imaging. 2010 Aug;37 Suppl 1:S164-82.

3. Nielsen T, Wittenborn T, Horsman MR. Dynamic Contrast-Enhanced Magnetic Resonance Imaging (DCE-MRI) in Preclinical Studies of Antivascular Treatments. Pharmaceutics. 2012;4(4):563-89.

4. Ferl GZ, Port RE. Quantification of antiangiogenic and antivascular drug activity by kinetic analysis of DCE-MRI data. Clin Pharmacol Ther. 2012 Jul;92(1):118-24.

5. Sourbron SP, Buckley DL. Tracer kinetic modelling in MRI: estimating perfusion and capillary permeability. Phys Med Biol. 2012 Jan 21;57(2):R1-33.

6. Sourbron SP, Buckley DL. Classic models for dynamic contrast-enhanced MRI. NMR Biomed. 2013 Aug;26(8):1004-27.

7. Tofts PS, Kermode AG. Measurement of the blood-brain barrier permeability and leakage space using dynamic MR imaging. 1. Fundamental concepts. Magn Reson Med. 1991 Feb;17(2):357-67.

8. Tofts PS. Modeling tracer kinetics in dynamic Gd-DTPA MR imaging. J Magn Reson Imaging. 1997 Jan-Feb;7(1):91-101.

9. Tofts PS, Brix G, Buckley DL, Evelhoch JL, Henderson E, Knopp MV, et al. Estimating kinetic parameters from dynamic contrast-enhanced T1-weighted MRI of a

diffusable tracer: standardized quantities and symbols. J Magn Reson Imaging. 1999 Sep;10(3):223-32.

10. Sourbron SP, Buckley DL. On the scope and interpretation of the Tofts models for DCE-MRI. Magn Reson Med. 2011 Sep;66(3):735-45.

11. Siemann DW. The unique characteristics of tumor vasculature and preclinical evidence for its selective disruption by Tumor-Vascular Disrupting Agents. Cancer Treat Rev. 2011 Feb;37(1):63-74.

12. Tozer GM, Prise VE, Wilson J, Cemazar M, Shan S, Dewhirst MW, et al. Mechanisms associated with tumor vascular shut-down induced by combretastatin A-4 phosphate: intravital microscopy and measurement of vascular permeability. Cancer Res. 2001 Sep 1;61(17):6413-22.

13. Baguley BC, Siemann DW. Temporal aspects of the action of ASA404 (vadimezan; DMXAA). Expert Opin Investig Drugs. 2010 Nov;19(11):1413-25.

14. de Lussanet QG, Langereis S, Beets-Tan RG, van Genderen MH, Griffioen AW, van Engelshoven JM, et al. Dynamic contrast-enhanced MR imaging kinetic parameters and molecular weight of dendritic contrast agents in tumor angiogenesis in mice. Radiology. 2005 Apr;235(1):65-72.

15. Jaspers K, Aerts HJ, Leiner T, Oostendorp M, van Riel NA, Post MJ, et al. Reliability of pharmacokinetic parameters: small vs. medium-sized contrast agents. Magn Reson Med. 2009 Sep;62(3):779-87.

16. Lemasson B, Serduc R, Maisin C, Bouchet A, Coquery N, Robert P, et al. Monitoring blood-brain barrier status in a rat model of glioma receiving therapy: dual injection of low-molecular-weight and macromolecular MR contrast media. Radiology. 2010 Nov;257(2):342-52.

17. Orth RC, Bankson J, Price R, Jackson EF. Comparison of single- and dual-tracer pharmacokinetic modeling of dynamic contrast-enhanced MRI data using low, medium, and high molecular weight contrast agents. Magn Reson Med. 2007 Oct;58(4):705-16.

18. Henderson E, Sykes J, Drost D, Weinmann HJ, Rutt BK, Lee TY. Simultaneous MRI measurement of blood flow, blood volume, and capillary permeability in mammary tumors using two different contrast agents. J Magn Reson Imaging. 2000 Dec;12(6):991-1003.

19. Jacobs I, Strijkers GJ, Keizer HM, Janssen HM, Nicolay K, Schabel MC. A novel approach to tracer-kinetic modeling for (macromolecular) dynamic contrast-enhanced MRI. Magn Reson Med. 2016 Apr 4;75(3):1142-53.

20. Zhao L, Ching LM, Kestell P, Kelland LR, Baguley BC. Mechanisms of tumor vascular shutdown induced by 5,6-dimethylxanthenone-4-acetic acid (DMXAA): Increased tumor vascular permeability. Int J Cancer. 2005 Aug 20;116(2):322-6.

21. Dowell NG, Tofts PS. Fast, accurate, and precise mapping of the RF field in vivo using the 180 degrees signal null. Magn Reson Med. 2007 Sep;58(3):622-30.

22. Schabel MC, DiBella EV, Jensen RL, Salzman KL. A model-constrained Monte Carlo method for blind arterial input function estimation in dynamic contrast-enhanced MRI: II. In vivo results. Phys Med Biol. 2010 Aug 21;55(16):4807-23.

23. Schabel MC, Fluckiger JU, DiBella EV. A model-constrained Monte Carlo method for blind arterial input function estimation in dynamic contrast-enhanced MRI: I. Simulations. Phys Med Biol. 2010 Aug 21;55(16):4783-806.

24. Schabel MC. A unified impulse response model for DCE-MRI. Magn Reson Med. 2012 Nov;68(5):1632-46.

25. Beaumont M, Lemasson B, Farion R, Segebarth C, Remy C, Barbier EL. Characterization of tumor angiogenesis in rat brain using iron-based vessel size index MRI in combination with gadolinium-based dynamic contrast-enhanced MRI. J Cereb Blood Flow Metab. 2009 Oct;29(10):1714-26.

26. Pike MM, Stoops CN, Langford CP, Akella NS, Nabors LB, Gillespie GY. High-resolution longitudinal assessment of flow and permeability in mouse glioma vasculature: Sequential small molecule and SPIO dynamic contrast agent MRI. Magn Reson Med. 2009 Mar;61(3):615-25.

27. Su MY, Muhler A, Lao X, Nalcioglu O. Tumor characterization with dynamic contrast-enhanced MRI using MR contrast agents of various molecular weights. Magn Reson Med. 1998 Feb;39(2):259-69.

28. Baguley BC. Antivascular therapy of cancer: DMXAA. Lancet Oncol. 2003 Mar;4(3):141-8.

29. Hofmann S, Grasberger H, Jung P, Bidlingmaier M, Vlotides J, Janssen OE, et al. The tumour necrosis factor-alpha induced vascular permeability is associated with a reduction of VE-cadherin expression. Eur J Med Res. 2002 Apr 30;7(4):171-6.

30. Seshadri M, Spernyak JA, Mazurchuk R, Camacho SH, Oseroff AR, Cheney RT, et al. Tumor vascular response to photodynamic therapy and the antivascular agent 5,6-dimethylxanthenone-4-acetic acid: implications for combination therapy. Clin Cancer Res. 2005 Jun 01;11(11):4241-50.

31. Lara PN, Jr., Douillard JY, Nakagawa K, von Pawel J, McKeage MJ, Albert I, et al. Randomized phase III placebo-controlled trial of carboplatin and paclitaxel with or without the vascular disrupting agent vadimezan (ASA404) in advanced non-small-cell lung cancer. J Clin Oncol. 2011 Aug 01;29(22):2965-71.

32. Albrecht M, Henke J, Tacke S, Markert M, Guth B. Influence of repeated anaesthesia on physiological parameters in male Wistar rats: a telemetric study about isoflurane, ketamine-xylazine and a combination of medetomidine, midazolam and fentanyl. BMC Vet Res. 2014 Dec 31;10:310.

33. Jain RK. Normalization of tumor vasculature: an emerging concept in antiangiogenic therapy. Science. 2005 Jan 7;307(5706):58-62.

34. Ferrara N, Adamis AP. Ten years of anti-vascular endothelial growth factor therapy. Nat Rev Drug Discov. 2016 Jun;15(6):385-403.

35. Schabel MC, Gilbert E, Guimaraes A, Wyatt C. Physiologically-constrained Multiagent DCE-MRI for Pancreatic Cancer Imaging. Proceedings of ISMRM 25th Annual Meeting, Honolulu, HI. 2017.

Figure legends

Figure 1. Multi-agent DCE-MRI parameter maps before and longitudinally after DXMAA treatment. Representative multi-agent DCE-MRI parameter maps of an animal treated with DMXAA. The parameter maps in the tumor tissue are superimposed on the anatomical T_2-weighted image. The maps are colored according to the color bar on the right-hand side of the plot. The corresponding parameter range for this scale bar is shown above each column of panels. The white tumor pixels represent non-perfused pixels. After treatment, a large portion of the tumor was non-perfused. In the remaining perfused area, a pronounced decrease in flow was observed at both 2 h and 24 h after treatment. The extraction fraction, particularly of G5 and G2, initially increased at 2 h after treatment and then restored again to baseline values at 24 h after treatment. The increased permeability was not reflected in the K^{trans} values due to the confounding influence of diminished blood flow.

E: extraction fraction; F: blood flow; K^{trans}: transfer constant

Figure 2. Multi-agent DCE-MRI parameter maps before and longitudinally after placebo treatment. Representative multi-agent DCE-MRI parameter maps of an animal treated with placebo. The parameter maps in the tumor tissue are superimposed on the anatomical T_2-weighted image. The maps are colored according to the color bar on the right-hand side of the plot. The corresponding parameter range for this scale bar is shown above each column of panels. The white tumor pixels represent non-perfused pixels. The DCE-MRI parameters did not show differences between the time points.

E: extraction fraction; F: blood flow; K^{trans}: transfer constant

Figure 3. Treatment-induced changes in multi-agent DCE-MRI parameters. Mean ± SD multi-agent DCE-MRI parameter values over time in the perfused pixels of the DMXAA-treated (solid line) and placebo-treated (dashed line) tumors. * and ** represent a significant difference compared to baseline with P<0.05 and P<0.001, respectively. ## represents a significant difference compared to 2 h after treatment with P<0.001. α^{-1}: vascular heterogeneity index; E: extraction fraction; F: blood flow; K^{trans}: transfer constant; PF: perfused fraction; t_c: mean capillary transit time; v_b = blood volume fraction; v_e = extravascular extracellular volume fraction

Figure 4. Treatment-induced changes in histological measurements of the tumor vasculature. A) Histological images of a tumor section of a mouse sacrificed 2 hours after placebo treatment (left) and a mouse sacrificed 2 hours after DMXAA treatment (right). The scale bars represent 1 mm. Zoomed images of the regions indicated with the white rectangles are shown at the bottom row. The blue signal originates from the Hoechst dye and represents perfusion. The red signal originates from the endothelium staining and represents vasculature. In the DMXAA-treated animals, large regions of non-perfused tumor tissue were observed. B) Bar charts of perfusion fraction (PF) and vascular density (VD) at 2 h and 24 h after placebo and DMXAA treatment. * indicates a significant difference in PF between placebo-treated and DMXAA-treated groups at 2 h after treatment (P=0.005). ## indicates a significant difference between placebo-treated and DMXAA-treated groups at 24 h after treatment (P<0.001).

Figure 1

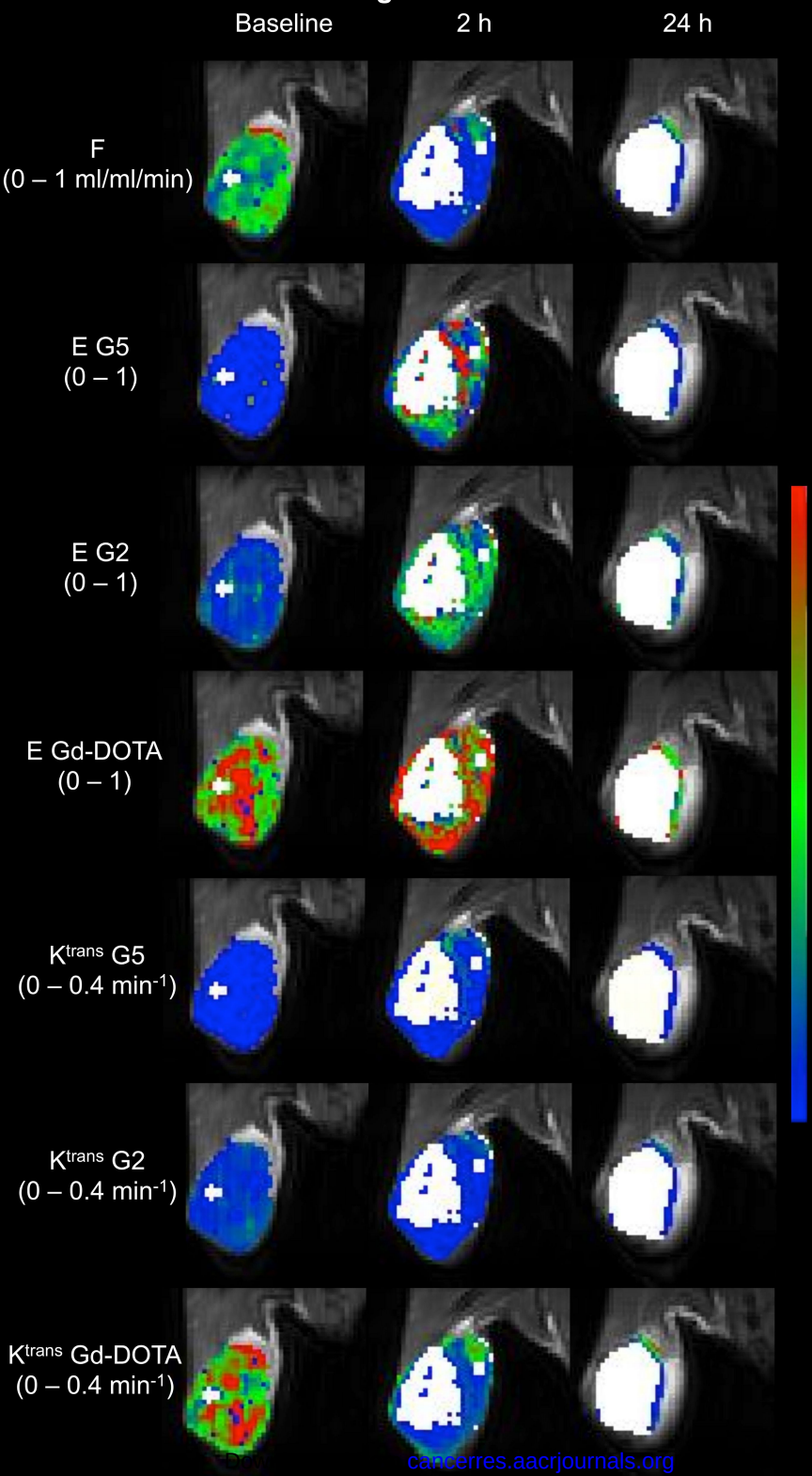

Figure 2

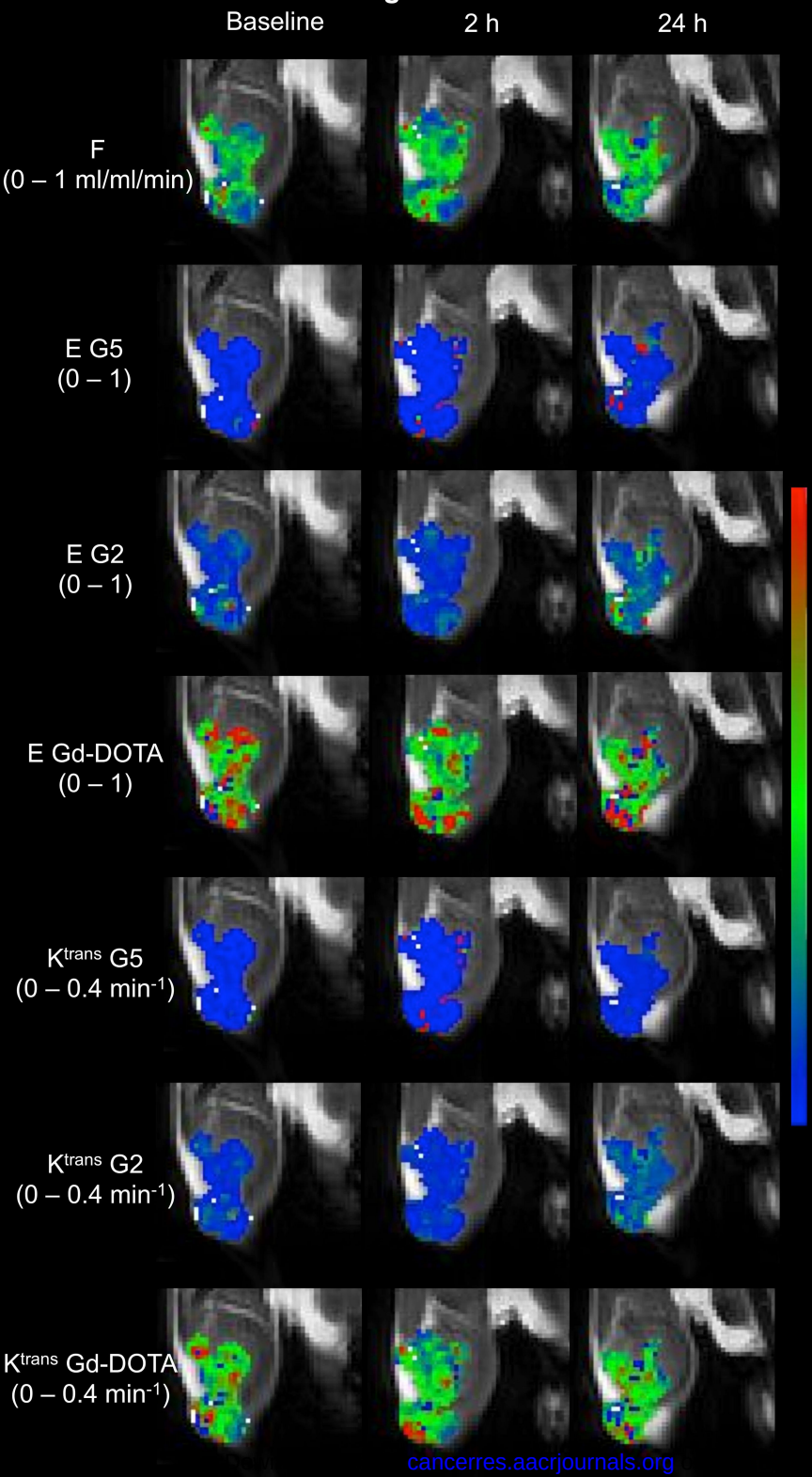

Figure 3

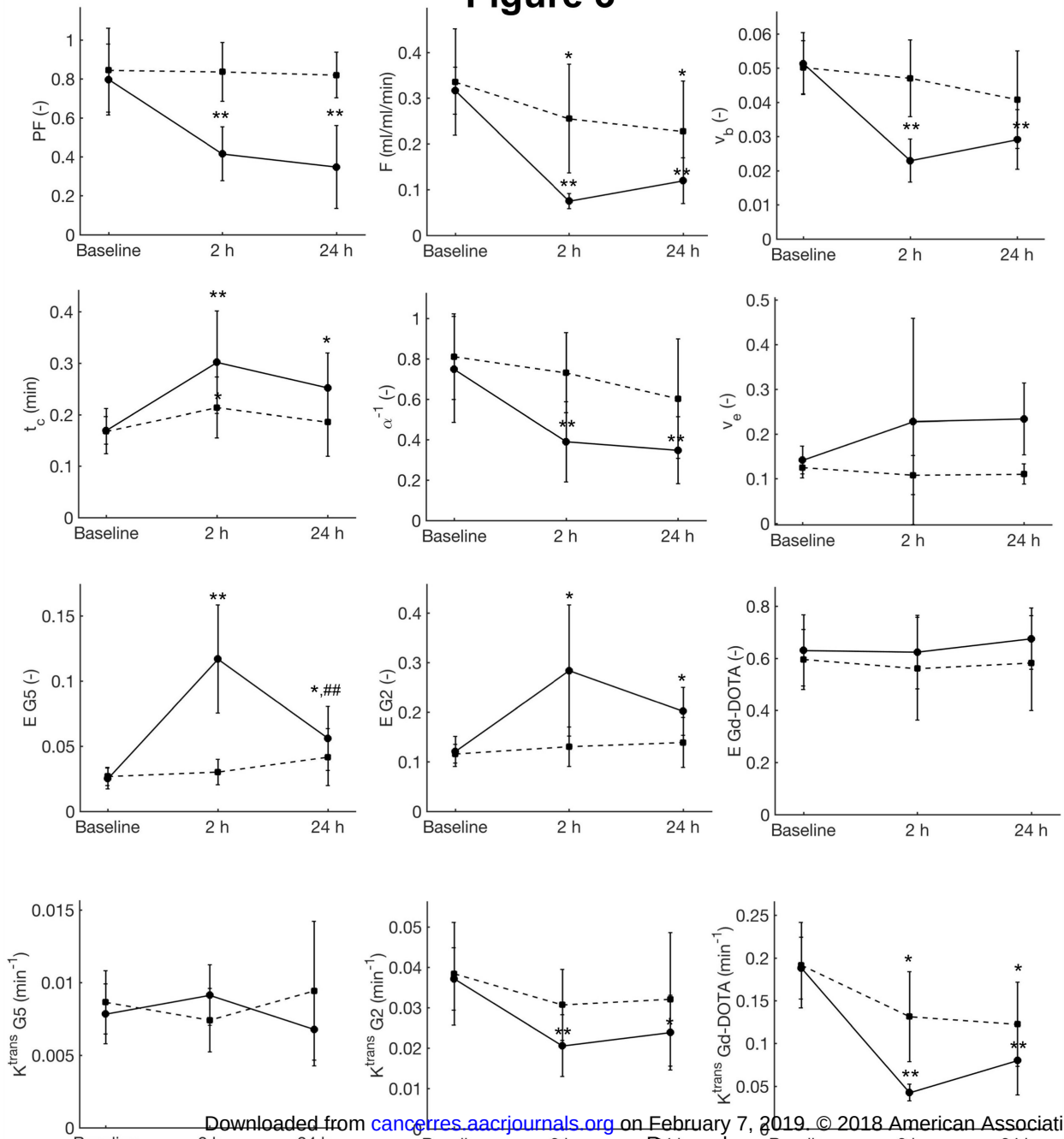

Figure 4

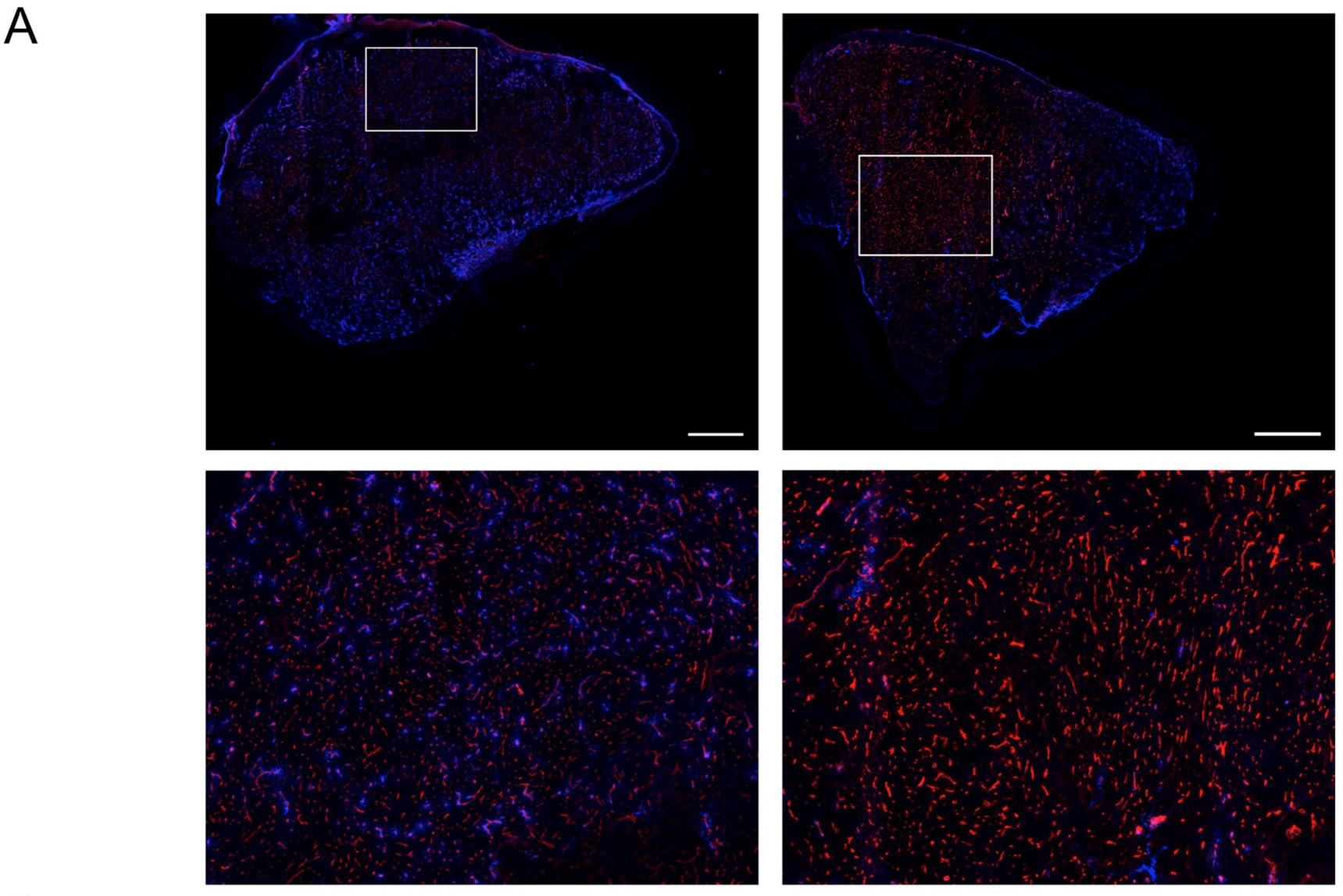

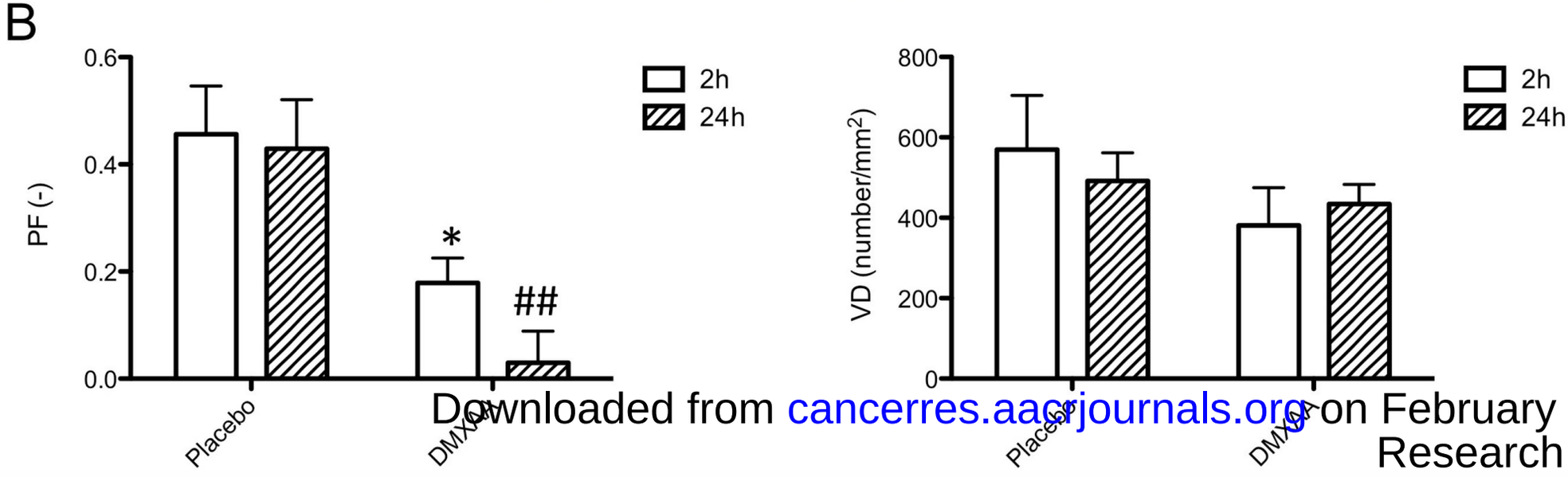

Cancer Research
The Journal of Cancer Research (1916–1930) | The American Journal of Cancer (1931–1940)

AACR American Association for Cancer Research

Improved evaluation of antivascular cancer therapy using constrained tracer-kinetic modeling for multi-agent dynamic contrast-enhanced MRI

Stefanie Hectors, Igor Jacobs, Jasper Lok, et al.

Cancer Res Published OnlineFirst January 9, 2018.